Author(s): Hinkkanen, Marko & Repo, Anna-Kaisa & Luomi, Jorma

Title: Influence of magnetic saturation on induction motor model selection

Year: 2006

Version: Post print

Please cite the original version:

Hinkkanen, Marko & Repo, Anna-Kaisa & Luomi, Jorma. 2006. Influence of magnetic saturation on induction motor model selection. XVII International Conference on Electrical Machines (ICEM2006). 6.

Influence of Magnetic Saturation on Induction Motor Model Selection

Marko Hinkkanen, Anna-Kaisa Repo, and Jorma Luomi

***Abstract*—Effects of magnetic saturation on various equivalent circuit models of an induction motor are studied. The parameters of 2.2-kW and 37-kW motors with closed rotor slots are analyzed using finite element computations. Both skewed and unskewed rotor slots are studied. The magnetizing inductance not only depends on the main flux, but is also dependent on the rotor current, especially if the rotor slots are skewed or closed. The stator leakage inductance is essentially constant, while the rotor leakage inductance depends significantly on the rotor current. The performance of vector-controlled drives can be improved by using a T or Γ-equivalent circuit model whose inductances also depend on the rotor current.**

***Index Terms*—Closed slots, induction motors, magnetic saturation, motor models, rotor skew.**

I. Introduction

Induction motors are usually saturated in the rated operating point. Typically, small motors have skewed and closed rotor slots, increasing the complexity of the saturation phenomena. In induction motor drives, the accuracy of the torque production depends on the dynamic motor model used in the estimation and control algorithms. The model is usually illustrated by a dynamic equivalent circuit. It is difficult to identify the leakage inductances of the ordinary T model by means of practical measurements. Therefore, transformations leading to the Γ model or the inverse-Γ model are often preferred [1].

The resistances of the T model depend only on the temperature at usual slip frequencies, while the inductances vary strongly with the operating point. Conventionally, the magnetizing inductance is assumed to saturate as a function of the main flux (air-gap flux). However, it has been observed that the magnetizing inductance may also depend on the electromagnetic torque (or the rotor current) [2]. This dependency originates from skewed rotor slots [3], saturation of stator tooth tips and rotor surface at high stator and rotor currents, and flux lines crossing the slots [4]. Furthermore, if the rotor slots are closed, the rotor leakage inductance saturates significantly as a function of the rotor current [5]. The effects of the saturation become more complicated when the Γ or inverse-Γ model is considered.

This paper deals with model parameters in operating points typical of controlled induction motor drives. Equivalent-circuit parameters describing the fundamental-wave behavior of the T model are evaluated using a finite element (FE) method. The effect of the rotor skew on the parameters is clarified by analyzing both skewed and unskewed motors. Finally, the variation of the Γ and inverse-Γ model parameters is analyzed.

This work was supported in part by ABB Oy. The contribution of Prof. A. Arkkio is gratefully acknowledged.

M. Hinkkanen and J. Luomi are with the Power Electronics Laboratory, Helsinki University of Technology, FI-02015 TKK, Finland (e-mail: marko.hinkkanen@tkk.fi; jorma.luomi@tkk.fi).

A.-K. Repo is with the Laboratory of Electromechanics, Helsinki University of Technology, FI-02015 TKK, Finland (e-mail: anna-kaisa.repo@tkk.fi).

II. Models

The three flux linkage models of the induction motor shown in Fig. 1 are mathematically equivalent for constant parameters. The conventional T model is commonly used in the literature, but the simpler inverse-Γ model is more suitable for control purposes.

A. T Model

The voltage equations of the induction motor are in a general reference frame

$$\underline{u}_\mathrm{s} = R_\mathrm{s}\underline{i}_\mathrm{s} + \frac{\mathrm{d}\underline{\psi}_\mathrm{s}}{\mathrm{d}t} + \mathrm{j}\omega_\mathrm{k}\underline{\psi}_\mathrm{s} \tag{1}$$

$$0 = R_\mathrm{r}\underline{i}_\mathrm{r} + \frac{\mathrm{d}\underline{\psi}_\mathrm{r}}{\mathrm{d}t} + \mathrm{j}\left(\omega_\mathrm{k} - \omega_\mathrm{m}\right)\underline{\psi}_\mathrm{r} \tag{2}$$

where $\underline{u}_\mathrm{s}$ is the space vector of the stator voltage, R_s the stator resistance, $\underline{i}_\mathrm{s}$ the stator current vector, and ω_k the angular speed of the reference frame. The rotor resistance is R_r, the rotor current vector $\underline{i}_\mathrm{r}$, and the electrical angular speed of the rotor ω_m. The stator and rotor flux linkage vectors are

$$\underline{\psi}_\mathrm{s} = L_\mathrm{s}\underline{i}_\mathrm{s} + L_\mathrm{m}\underline{i}_\mathrm{r}, \quad \underline{\psi}_\mathrm{r} = L_\mathrm{m}\underline{i}_\mathrm{s} + L_\mathrm{r}\underline{i}_\mathrm{r} \tag{3}$$

respectively. The stator and rotor inductances are defined by $L_\mathrm{s} = L_\mathrm{m} + L_{\mathrm{s}\sigma}$ and $L_\mathrm{r} = L_\mathrm{m} + L_{\mathrm{r}\sigma}$, respectively, where $L_{\mathrm{s}\sigma}$ and $L_{\mathrm{r}\sigma}$ are the stator and rotor leakage inductances, respectively, and L_m is the magnetizing inductance. The flux linkage model corresponding to (3) is shown in Fig. 1(a), where the magnetizing current $\underline{i}_\mathrm{m} = \underline{i}_\mathrm{s} + \underline{i}_\mathrm{r}$ and the main flux linkage $\underline{\psi}_\mathrm{m} = L_\mathrm{m}\underline{i}_\mathrm{m}$ are also depicted. For per-unit quantities, the electromagnetic torque is given by

$$T_\mathrm{e} = \mathrm{Im}\{\underline{i}_\mathrm{s}\underline{\psi}_\mathrm{s}^*\} = \mathrm{Im}\{\underline{\psi}_\mathrm{r}\underline{i}_\mathrm{r}^*\} \tag{4}$$

where the complex conjugate is marked by the symbol *.

B. Inverse-Γ Model

The number of model parameters can be decreased from five to four by scaling the rotor flux linkage as $\underline{\psi}_\mathrm{R} = k_\mathrm{r}\underline{\psi}_\mathrm{r}$ and the rotor current as $\underline{i}_\mathrm{R} = \underline{i}_\mathrm{r}/k_\mathrm{r}$, where the magnetic coupling factor of the rotor is defined by $k_\mathrm{r} = L_\mathrm{m}/L_\mathrm{r}$. Furthermore, the scaled magnetizing inductance $L_\mathrm{M} = k_\mathrm{r}L_\mathrm{m}$, the scaled

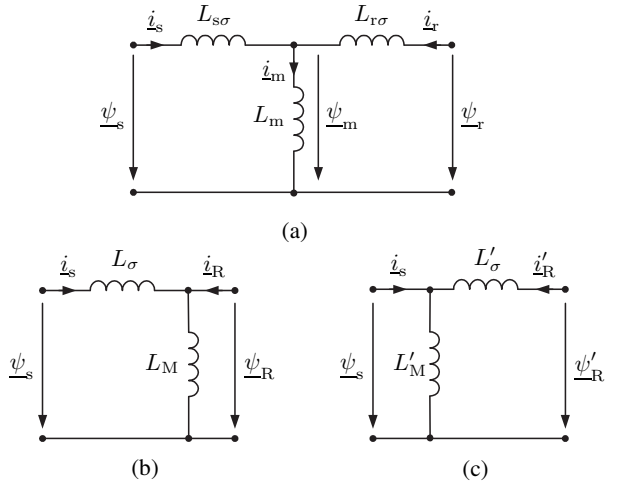

Fig. 1. Flux linkage models: (a) T model; (b) inverse-Γ model; (c) Γ model.

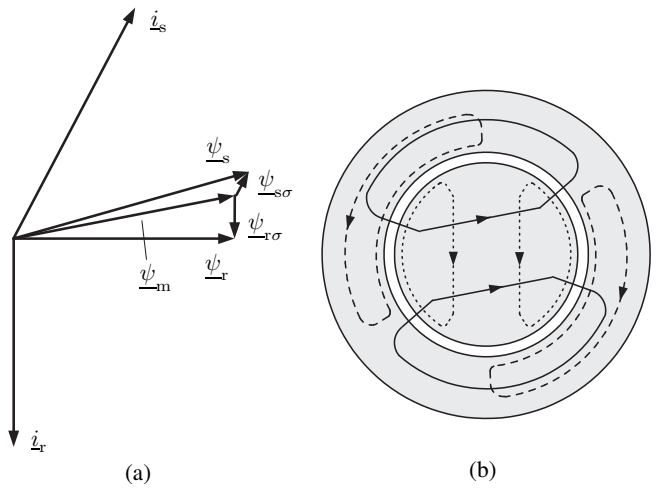

Fig. 2. (a) Space vector diagram and (b) magnetic flux paths: main flux (solid), stator leakage flux (dashed), and rotor leakage flux (dotted).

rotor resistance $R_\mathrm{R} = k_\mathrm{r}^2 R_\mathrm{r}$, and the total leakage inductance $L_\sigma = L_{\mathrm{s}\sigma} + k_\mathrm{r} L_{\mathrm{r}\sigma}$ are introduced. Now the rotor voltage equation (2) becomes

$$0 = R_\mathrm{R}\underline{i}_\mathrm{R} + \frac{\mathrm{d}\underline{\psi}_\mathrm{R}}{\mathrm{d}t} + \mathrm{j}\,(\omega_\mathrm{k} - \omega_\mathrm{m})\,\underline{\psi}_\mathrm{R} \tag{5}$$

and the flux linkage equations (3) become

$$\underline{\psi}_\mathrm{s} = (L_\sigma + L_\mathrm{M})\,\underline{i}_\mathrm{s} + L_\mathrm{M}\underline{i}_\mathrm{R}, \quad \underline{\psi}_\mathrm{R} = L_\mathrm{M}\,(\underline{i}_\mathrm{s} + \underline{i}_\mathrm{R}) \tag{6}$$

The flux linkage model corresponding to (6) is shown in Fig. 1(b). Equations (1) and (4) remain unchanged for the inverse-Γ model.

C. Γ Model

Alternatively, the number of model parameters can be decreased from five to four by choosing $\underline{\psi}'_\mathrm{R} = \underline{\psi}_\mathrm{r}/k_\mathrm{s}$ and $\underline{i}'_\mathrm{R} = k_\mathrm{s}\underline{i}_\mathrm{r}$, where the magnetic coupling factor of the stator is defined by $k_\mathrm{s} = L_\mathrm{m}/L_\mathrm{s}$. Furthermore, the parameters $R'_\mathrm{R} = R_\mathrm{r}/k_\mathrm{s}^2$, $L'_\mathrm{M} = L_\mathrm{m}/k_\mathrm{s}$, and $L'_\sigma = L_{\mathrm{s}\sigma}/k_\mathrm{s} + L_{\mathrm{r}\sigma}/k_\mathrm{s}^2$ are introduced. The flux linkage equations are

$$\underline{\psi}_\mathrm{s} = L'_\mathrm{M}\,(\underline{i}_\mathrm{s} + \underline{i}'_\mathrm{R}), \quad \underline{\psi}'_\mathrm{R} = L'_\mathrm{M}\underline{i}_\mathrm{s} + (L'_\sigma + L'_\mathrm{M})\,\underline{i}'_\mathrm{R} \tag{7}$$

corresponding to Fig. 1(c). The variables and parameters of the rotor voltage equation (2) are replaced with the scaled quantities defined above. Equations (1) and (4) remain unchanged.

III. Overview of Magnetic Saturation

A. Main Flux and Leakage Fluxes

A vector diagram showing fluxes and currents of the T model is depicted in Fig. 2(a), where the rotor leakage flux is $\underline{\psi}_{\mathrm{r}\sigma} = L_{\mathrm{r}\sigma}\underline{i}_\mathrm{r}$ and the stator leakage flux $\underline{\psi}_{\mathrm{s}\sigma} = L_{\mathrm{s}\sigma}\underline{i}_\mathrm{s}$. The main flux path, the rotor leakage flux path, and the stator leakage flux path are sketched in the motor cross-section in Fig. 2(b). The main flux causes saturation principally in the teeth and yokes of the stator and the rotor.

In the case of closed rotor slots, the slot bridges provide a path for the rotor leakage flux. The rotor leakage inductance $L_{\mathrm{r}\sigma}$ saturates strongly as a function of the rotor current [6], [7]. The rotor flux is smaller than the main flux due to the rotor leakage flux since $\psi_\mathrm{r} = \sqrt{\psi_\mathrm{m}^2 - L_{\mathrm{r}\sigma}^2 i_\mathrm{r}^2}$ in steady state. Thus, increasing the rotor current should decrease the saturation in the rotor teeth and yoke. However, the rotor leakage flux is nearly perpendicular to the main flux, and it can be noticed in Fig. 2(b) that the saturation at the rotor surface and in the slot bridges caused by the rotor leakage flux appears in the main flux path. Therefore, the magnetizing inductance L_m may saturate significantly as a function of the rotor leakage flux (or the rotor current), particularly if the rotor slots are closed.

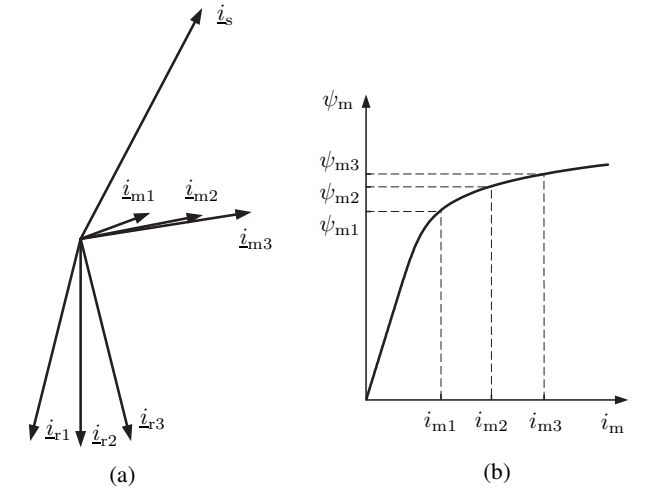

Fig. 3. Effect of skewed rotor when the motor consists of three slices with different rotor positions: (a) current space vectors and (b) saturation characteristics. Currents in the end slices are marked by subscripts 1 and 3 and currents in the middle slice by the subscript 2.

If the stator slots are semi-closed (or open) as usual, the saturation of the stator leakage inductance $L_{\mathrm{s}\sigma}$ is insignificant unless the current is very high. The stator leakage flux increases the load dependency of L_m only slightly.

B. Rotor Skewing

Assuming linear magnetic properties, skewing the rotor slots increases the rotor resistance and the rotor leakage inductance [8]. When the magnetic saturation is taken into account, the

TABLE I
MOTOR RATING

Power (kW)	2.2	37
Speed (r/min)	1 430	1 470
Frequency f_{N} (Hz)	50	50
Line-to-line voltage U_{N} (V, rms)	400	380
Current I_{N} (A, rms)	5.0	73

rotor skew also has an influence on the magnetizing inductance [3]. A dominant effect is the change in the relative phase of the stator and rotor currents in the axial direction due to the skewed rotor bars, causing the saturation level of a loaded motor to vary in the axial direction. A skewed motor can be considered to consist of an infinite number of elemental machines lying in radial planes and connected in series, with a gradual relative phase shift between the stator and rotor currents in the axial direction [9]. The motor is assumed to consist of three slices in Fig. 3(a), where the rotor current vectors are $\underline{i}_{\mathrm{r}1}$, $\underline{i}_{\mathrm{r}2}$, and $\underline{i}_{\mathrm{r}3}$ and the magnetizing current vectors are $\underline{i}_{\mathrm{m}1} = \underline{i}_{\mathrm{s}} + \underline{i}_{\mathrm{r}1}$, $\underline{i}_{\mathrm{m}2} = \underline{i}_{\mathrm{s}} + \underline{i}_{\mathrm{r}2}$, and $\underline{i}_{\mathrm{m}3} = \underline{i}_{\mathrm{s}} + \underline{i}_{\mathrm{r}3}$. The effect of magnetic saturation on the corresponding flux linkages $\psi_{\mathrm{m}1}$, $\psi_{\mathrm{m}2}$, and $\psi_{\mathrm{m}3}$ is illustrated in Fig. 3(b). If a skewed motor is saturated, the magnetizing inductance

$$L_{\mathrm{m}} = \frac{\psi_{\mathrm{m}1} + \psi_{\mathrm{m}2} + \psi_{\mathrm{m}3}}{i_{\mathrm{m}1} + i_{\mathrm{m}2} + i_{\mathrm{m}3}} \tag{8}$$

becomes a function of the rotor current and decreases as the rotor current increases.

IV. ANALYSIS OF PARAMETER VARIATIONS

Parameter variations of 2.2-kW and 37-kW induction motors were analyzed in different steady-state operating points by means of a two-dimensional multi-slice FE method [10]. The motor rating is given in Table I. Both motors have closed rotor slots and semi-closed stator slots. Both skewed and unskewed rotors were studied. The skewed motors were assumed to be made up of six slices with different rotor positions. In the FE method, the time-dependence was approximately represented by sinusoidally varying quantities, and the magnetic saturation of iron was modeled using an effective reluctivity curve [11]. Furthermore, the iron losses were omitted. The parameters of the T model were evaluated from the results of the FE analysis.

The FE analysis was carried out at the constant stator frequency of $\omega_{\mathrm{s}} = 0.5$ p.u., while the magnitude of the stator voltage and the slip frequency ω_{r} were varied. At constant frequency and stator temperature (here 20°C), the stator resistance R_{s} can be assumed to be constant. A comparison between the calculated and measured currents for the skewed 2.2-kW motor can be found in the Appendix.

In Figs. 4–7, the calculated parameters are depicted as a function of the rotor flux magnitude ψ_{r} and the rotor current magnitude i_{r}. This choice is preferred due to the orthogonality of $\underline{\psi}_{\mathrm{r}}$ and $\underline{i}_{\mathrm{r}}$ in steady state. The constant rotor flux and constant rotor current curves were obtained using linear interpolation. It is to be noted that Figs. 4–7 change only slightly if they are plotted as a function of the main flux magnitude ψ_{m} and the rotor current magnitude i_{r}.

A. 2.2-kW Motor

The stator resistance of the 2.2-kW motor is R_{s} = 0.063 p.u., the number of stator slots is 36, the number of rotor slots 26, and the rotor skew is 1.38 stator slot pitches. In the rated operating point, the magnitudes of the rotor flux and the rotor current are $\psi_{\mathrm{r}} = 0.90$ p.u. and $i_{\mathrm{r}} = 0.76$ p.u., respectively. Figs. 4(a) and (b) show the magnetizing inductance L_{m} as a function of the rotor flux ψ_{r} and the rotor current i_{r}, respectively. It can be seen that L_{m} decreases almost linearly as a function of i_{r}. Figs. 4(c) and (d) show the rotor leakage inductance $L_{\mathrm{r}\sigma}$ as a function of ψ_{r} and i_{r}, respectively. The rotor leakage inductance $L_{\mathrm{r}\sigma}$ saturates strongly as a function of i_{r} when the flux is low. For the small values of the rotor current i_{r}, the inductance $L_{\mathrm{r}\sigma}$ also depends on the flux. This kind of saturation characteristics are due to the closed rotor slots; a comparably small rotor current or rotor flux causes saturation in the thin slot bridges. The stator leakage inductance and the rotor resistance are not shown since they are essentially constant in the given range of the rotor flux and rotor current ($L_{\mathrm{s}\sigma}$ = 0.05…0.07 p.u. and R_{r} = 0.037…0.039 p.u.).

In order to separate the effect of the skewed rotor, the parameters of the unskewed motor were also evaluated. The magnetizing inductance L_{m} shown in Fig. 5 is still a function of the rotor current i_{r}, but the dependency is reduced especially at higher flux levels. The saturation characteristics of the rotor leakage inductance $L_{\mathrm{r}\sigma}$ are similar to those of the skewed motor [Figs. 4(c) and (d)], except that $L_{\mathrm{r}\sigma}$ is slightly smaller.

B. 37-kW Motor

The stator resistance of the 37-kW motor is R_{s} = 0.021 p.u., the number of stator slots is 48, the number of rotor slots 40, and the rotor skew is 1.53 stator slot pitches. The magnitudes of the rotor flux and the rotor current in the rated operating point are $\psi_{\mathrm{r}} = 0.93$ p.u. and $i_{\mathrm{r}} = 0.87$ p.u., respectively. Figs. 6(a) and (b) show the magnetizing inductance L_{m} as a function of the rotor flux ψ_{r} and the rotor current i_{r}, respectively. Figs. 6(c) and (d) show the rotor leakage inductance $L_{\mathrm{r}\sigma}$ as a function of ψ_{r} and i_{r}, respectively. The effect of rotor current i_{r} on both L_{m} and $L_{\mathrm{r}\sigma}$ is even more significant than in the case of the 2.2-kW motor. In the studied operating range, the stator leakage inductance and the rotor resistance are nearly constant ($L_{\mathrm{s}\sigma}$ = 0.075…0.085 p.u. and R_{r} = 0.015…0.017 p.u.).

The parameters of the unskewed motor were also evaluated. The magnetizing inductance L_{m} is shown in Fig. 7. The saturation of L_{m} caused by the rotor current i_{r} is decreased compared to the skewed motor, but L_{m} still depends considerably on i_{r} even at higher flux levels. The rotor-current dependency of L_{m} is mainly caused by the saturation at the rotor surface and in the slot bridges due to the rotor leakage flux. This phenomenon was confirmed by analyzing the unskewed 37-kW motor equipped with semi-closed rotor slots; the variation of L_{m} as a function of i_{r} was reduced significantly and $L_{\mathrm{r}\sigma}$ was almost constant.

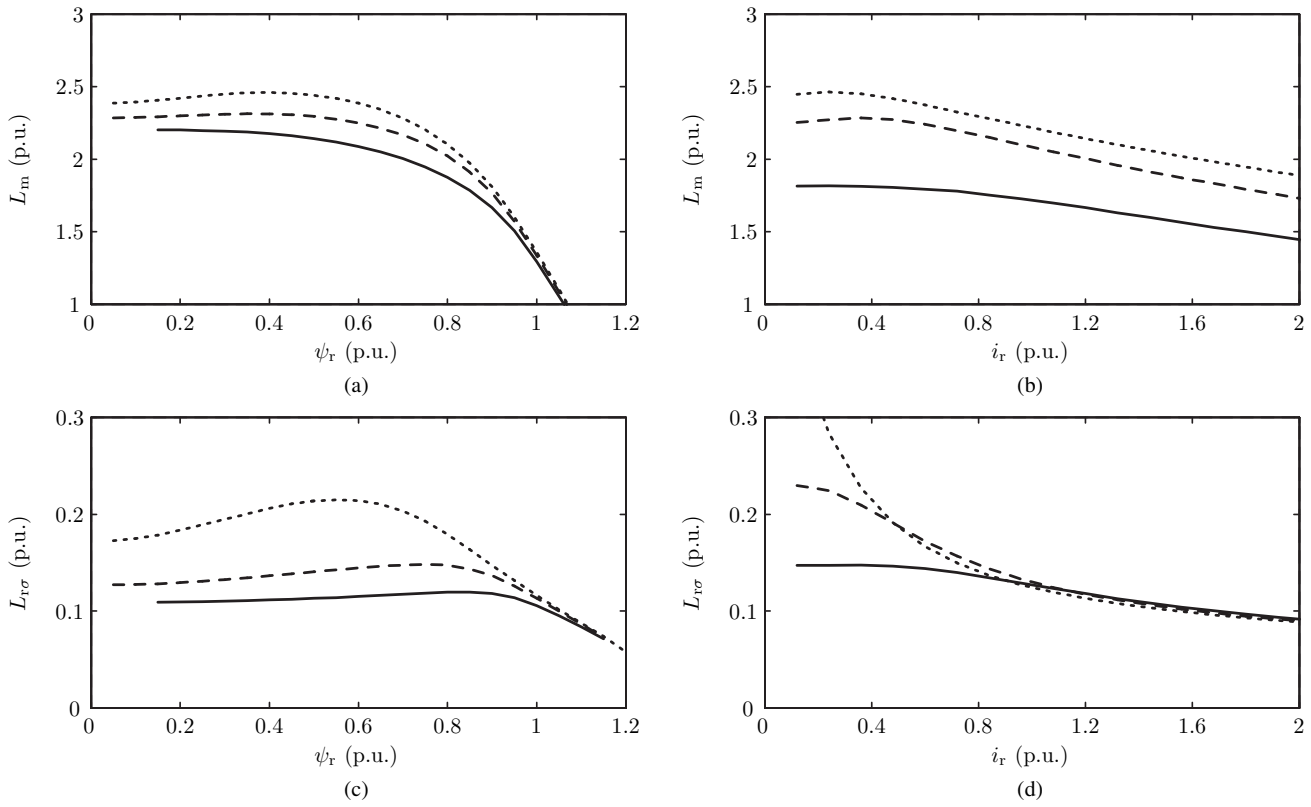

Fig. 4. Parameters for skewed 2.2-kW motor: (a) and (c) $i_\mathrm{r} = 0.4$ p.u. (dotted line), 0.8 p.u. (dashed), and 1.2 p.u. (solid); (b) and (d) $\psi_\mathrm{r} = 0.5$ p.u. (dotted line), 0.7 p.u. (dashed), and 0.9 p.u. (solid).

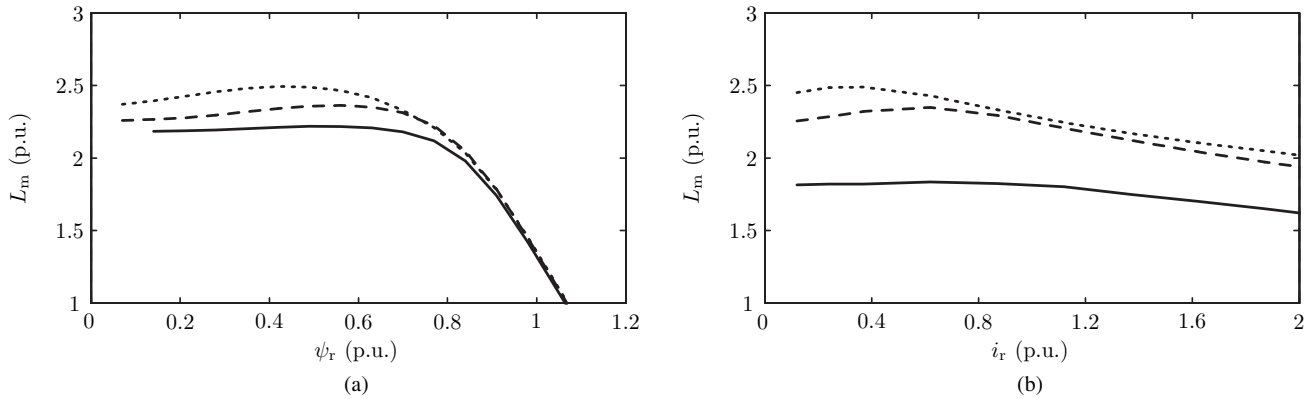

Fig. 5. Parameters for unskewed 2.2-kW motor: (a) $i_\mathrm{r} = 0.4$ p.u. (dotted line), 0.8 p.u. (dashed), and 1.2 p.u. (solid); (b) $\psi_\mathrm{r} = 0.5$ p.u. (dotted line), 0.7 p.u. (dashed), and 0.9 p.u. (solid).

V. Effects of Saturation on Controlled Drives

A. Rotor Flux Orientation

The principle of rotor flux orientation is briefly described here using the inverse-Γ model. The d-q reference frame is fixed to the actual rotor flux, i.e. $\omega_\mathrm{k} = \omega_\mathrm{s}$ and $\underline{\psi}_\mathrm{R} = \psi_\mathrm{R} + \mathrm{j}0$, where ω_s is the angular speed of the rotor flux. The dynamics of the rotor flux and the slip relation can be written as

$$\tau_\mathrm{r}\frac{\mathrm{d}\psi_\mathrm{R}}{\mathrm{d}t} + \psi_\mathrm{R} = L_\mathrm{M} i_\mathrm{sd}, \quad \omega_\mathrm{r} = \frac{R_\mathrm{R} i_\mathrm{sq}}{\psi_\mathrm{R}} \tag{9}$$

respectively, where the angular slip frequency is $\omega_\mathrm{r} = \omega_\mathrm{s} - \omega_\mathrm{m}$ and the rotor time constant is $\tau_\mathrm{r} = L_\mathrm{M}/R_\mathrm{R}$. The rotor flux magnitude is controlled using the d component i_sd of the stator current. The electromagnetic torque (4) can be expressed as

$$T_\mathrm{e} = \psi_\mathrm{R} i_\mathrm{sq} \tag{10}$$

If the rotor flux ψ_R is constant, the torque is proportional to the q component i_sq of the stator current. Equations (9) and (10) can be rewritten using the T model quantities; the desired constant relationship $T_\mathrm{e}/i_\mathrm{sq}$ is achieved only if $\psi_\mathrm{R} = k_\mathrm{r}\psi_\mathrm{r}$ is kept constant.

The motor model used in speed-sensored vector-controlled drives is usually based on (9) in some form. It can be shown that inaccurate parameter estimates result in an erroneous flux level and inaccurate torque production [12]. In sensorless drives, inaccurate parameter estimates may even cause stability

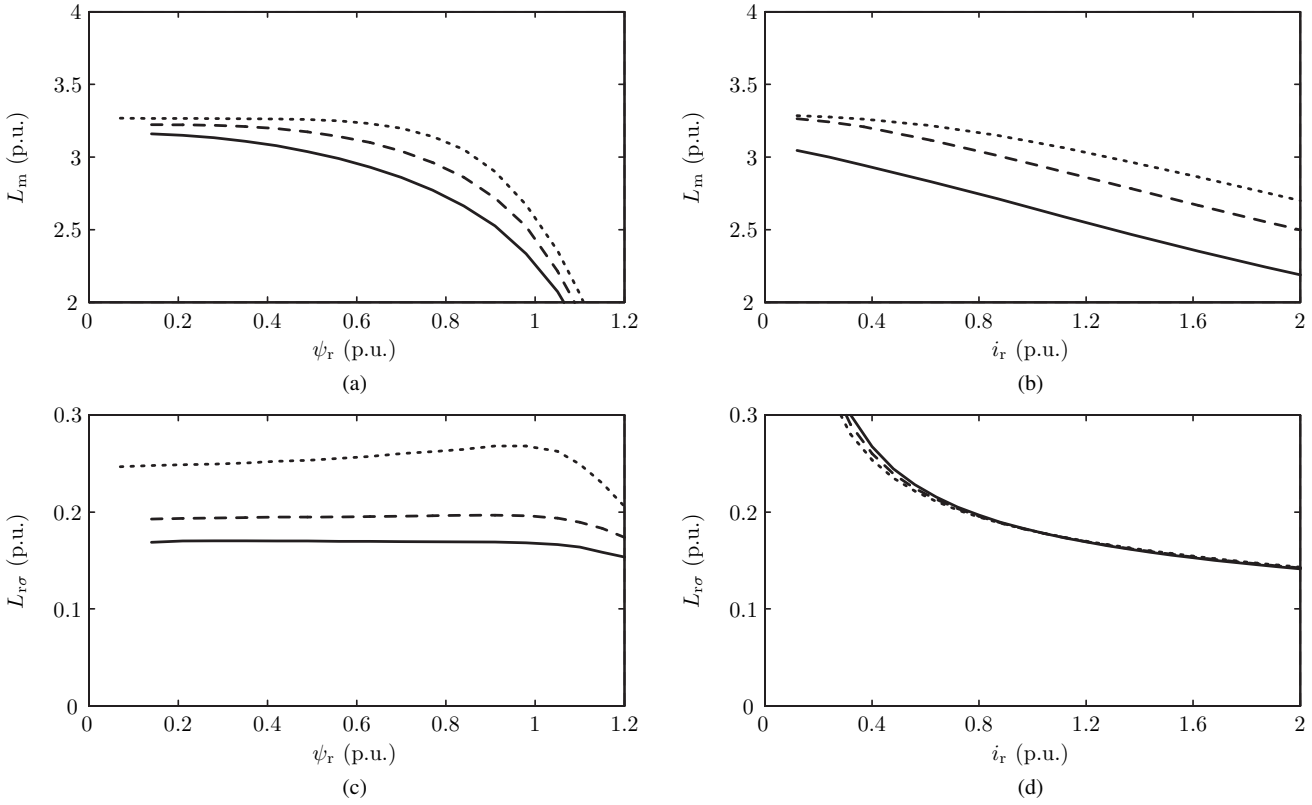

Fig. 6. Parameters for skewed 37-kW motor: (a) and (c) $i_\mathrm{r} = 0.4$ p.u. (dotted line), 0.8 p.u. (dashed), and 1.2 p.u. (solid); (b) and (d) $\psi_\mathrm{r} = 0.5$ p.u. (dotted line), 0.7 p.u. (dashed), and 0.9 p.u. (solid).

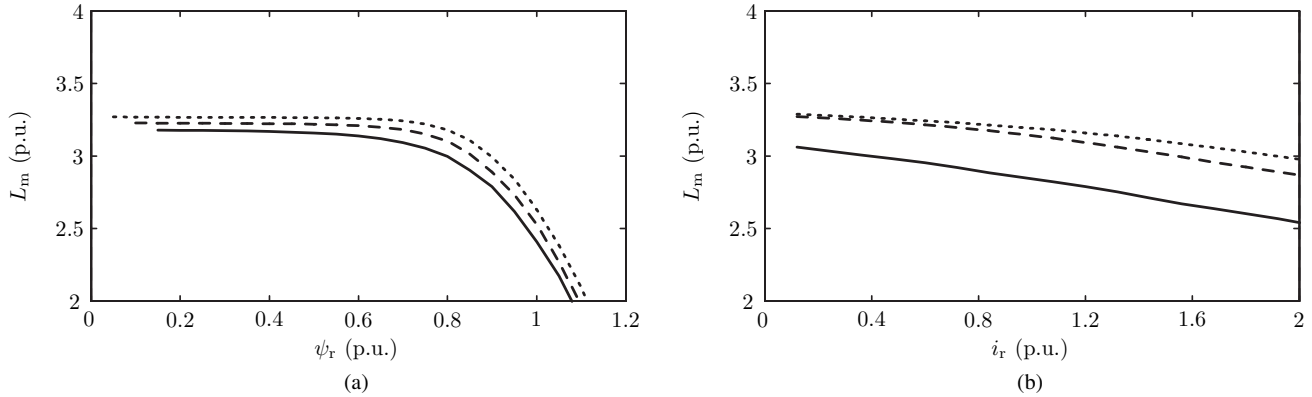

Fig. 7. Parameters for unskewed 37-kW motor: (a) $i_\mathrm{r} = 0.4$ p.u. (dotted line), 0.8 p.u. (dashed), and 1.2 p.u. (solid); (b) $\psi_\mathrm{r} = 0.5$ p.u. (dotted line), 0.7 p.u. (dashed), and 0.9 p.u. (solid).

problems. Hence, the performance of induction motor drives can be improved by incorporating the saturation effects caused by the rotor current into the motor model.

B. Model Selection

The parameters of the Γ and inverse-Γ models depend on the coupling factor k_s of the stator and the coupling factor k_r of the rotor, respectively. These factors are shown for the skewed 2.2-kW motor in Fig. 8. The coupling factor k_r depends strongly on the rotor current, contrary to k_s. Furthermore, the variation of k_r caused by the rotor flux is more complicated than that of k_s.

A disadvantage of the inverse-Γ model is the dependency of the rotor resistance $R_\mathrm{R} = k_\mathrm{r}^2 R_\mathrm{r}$ on the operating point, in addition to the effect of slowly changing temperature. Other inverse-Γ model parameters also behave inconsistently in the case of closed rotor slots. Hence, the parameter variations of the Γ model (or the T model) are generally easier to model than those of the inverse-Γ model. If rotor flux orientation is used, (9) and (10) can be rewritten for the Γ model, or the inverse-Γ model parameters can be easily calculated from those of the Γ model.

VI. Conclusions

The effects of closed rotor slots and rotor skew on the equivalent circuit parameters were analyzed using a FE method. The magnetizing inductance and the rotor leakage inductance depend significantly on the rotor current. To guarantee a good

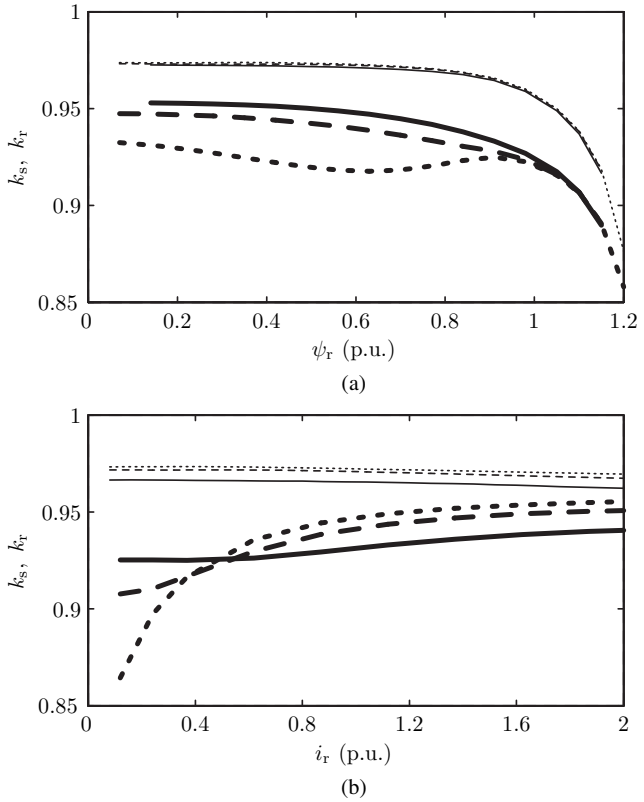

Fig. 8. Stator coupling factor k_s (thin lines) and rotor coupling factor k_r (thick) for skewed 2.2-kW motor: (a) $i_\mathrm{r} = 0.4$ p.u. (dotted line), 0.8 p.u. (dashed), and 1.2 p.u. (solid); (b) $\psi_\mathrm{r} = 0.5$ p.u. (dotted line), 0.7 p.u. (dashed), and 0.9 p.u. (solid).

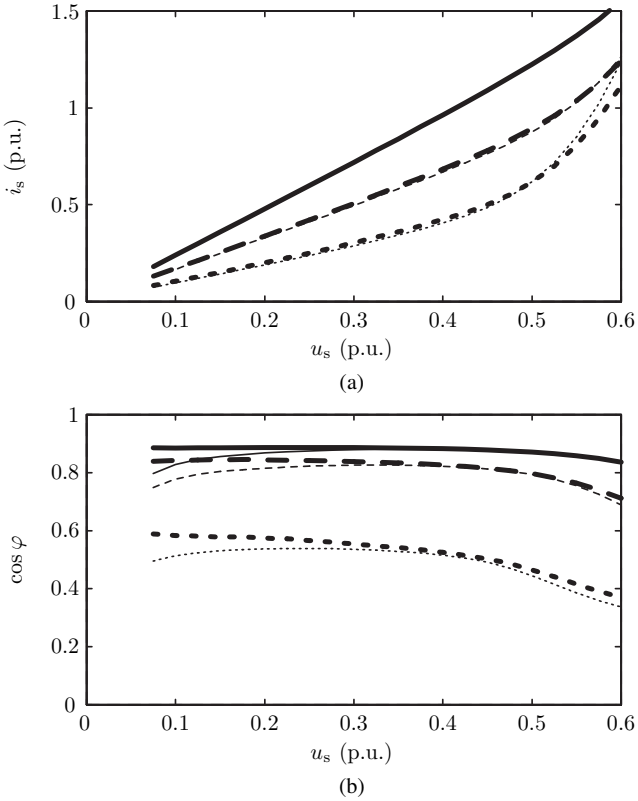

Fig. 9. Comparison between calculated (thin lines) and measured (thick) results for skewed 2.2-kW motor: (a) stator current magnitude; (b) power factor. Stator frequency $\omega_\mathrm{s} = 0.5$ p.u. and angular slip frequency $\omega_\mathrm{r} = 0.01$ p.u. (dotted line), 0.03 p.u. (dashed), and 0.05 p.u. (solid).

accuracy in the torque production, this dependency could be incorporated into the motor models of high-performance drives. The parameter variations of the Γ model are generally easier to model than those of the inverse-Γ model. Methods to identify the rotor-current dependency of the inductances is a suitable topic for future research.

Appendix
Comparison of Computed and Measured Results

Results of FE calculations for the skewed 2.2-kW motor are presented with the corresponding measured results in Fig. 9. The stator current magnitude i_s and the power factor $\cos\varphi$ are shown in Figs. 9(a) and (b), respectively, as a function of the stator voltage magnitude u_s at different angular slip frequencies ω_r. It can be seen that the results of FE calculations agree well with the measured results. The small difference in the power factor at low voltages may be related to the thickness of the rotor slot bridges, which is uncertain due to tolerances associated with the punching of the rotor sheets. Results of FE calculations for the 37-kW motor have been compared with measured results earlier [13].

References

[1] G. R. Slemon, "Modelling of induction machines for electric drives," *IEEE Trans. Ind. Appl.*, vol. 25, no. 6, pp. 1126–1131, Nov./Dec. 1989.

[2] M. Sumner and G. M. Asher, "Autocommissioning for voltage-referenced voltage-fed vector-controlled induction motor drives," *IEE Proc. B, Electr. Power Appl.*, vol. 140, no. 3, pp. 187–200, May 1993.

[3] C. Gerada, K. Bradley, M. Sumner, and P. Sewell, "Evaluation and modelling of cross saturation due to leakage flux in vector controlled induction machines," in *Proc. IEEE IEMDC'03*, vol. 3, Madison, WI, June 2003, pp. 1983–1989.

[4] J. Nerg, J. Pyrhönen, J. Partanen, and E. Ritchie, "Induction motor magnetizing inductance modelling as a function of torque," in *Proc. ICEM'04*, Cracow, Poland, Sept. 2004, CD-ROM.

[5] A. Yahiaoui and F. Bouillault, "Saturation effect on the electromagnetic behaviour of an induction machine," *IEEE Trans. Magn.*, vol. 31, no. 3, pp. 2036–2039, May 1995.

[6] T. S. Birch and O. I. Butler, "Permeance of closed-slot bridges and its effect on induction motor current computation," *Proc. IEE*, vol. 118, no. 1, pp. 169–172, Jan. 1971.

[7] S. Williamson and M. C. Begg, "Calculation of the bar resistance and leakage reactance of cage rotors with closed slots," *IEE Proc. B, Electr. Power Appl.*, vol. 132, no. 3, pp. 125–132, May 1985.

[8] O. I. Butler and T. S. Birch, "Comparison of alternative skew-effect parameters of cage induction motors," *Proc. IEE*, vol. 118, no. 7, pp. 879–883, July 1971.

[9] K. J. Binns, R. Hindmarsh, and B. P. Short, "Effect of skewing slots on flux distribution in induction machines," *Proc. IEE*, vol. 118, no. 3/4, pp. 543–549, Mar./Apr. 1971.

[10] A. Arkkio, "Analysis of induction motors based on the numerical solution of the magnetic field and circuit equations," Ph.D. dissertation, Dept. Elect. Commun. Eng., Helsinki Univ. Tech., Espoo, Finland, Dec. 1987. [Online]. Available: http://lib.tkk.fi/Diss/198X/isbn951226076X/

[11] J. Luomi, A. Niemenmaa, and A. Arkkio, "On the use of effective reluctivities in magnetic field analysis of induction motors fed from a sinusoidal voltage source," in *Proc. ICEM'86*, vol. 3, Munich, Germany, Sept. 1986, pp. 706–709.

[12] R. Krishnan and F. C. Doran, "Study of parameter sensitivity in high-performance inverter-fed induction motor drive systems," *IEEE Trans. Ind. Appl.*, vol. IA-23, no. 4, pp. 623–635, July/Aug. 1987.

[13] A. Arkkio, "Analysis of a 37 kW cage-induction motor," Helsinki University of Technology, Laboratory of Electromechanics, Espoo, Finland, Tech. Rep. 30, 1991.